Bulletin of Mathematical Biology (2010) 72: 1506–1533
DOI 10.1007/s11538-010-9507-6

ORIGINAL ARTICLE

Multiple Transmission Pathways and Disease Dynamics in a Waterborne Pathogen Model

Joseph H. Tien*, David J.D. Earn

Department of Mathematics and Statistics, McMaster University, Hamilton, Canada

Received: 15 August 2009 / Accepted: 15 January 2010 / Published online: 9 February 2010

Abstract Multiple transmission pathways exist for many waterborne diseases, including cholera, *Giardia*, *Cryptosporidium*, and *Campylobacter*. Theoretical work exploring the effects of multiple transmission pathways on disease dynamics is incomplete. Here, we consider a simple ODE model that extends the classical SIR framework by adding a compartment (W) that tracks pathogen concentration in the water. Infected individuals shed pathogen into the water compartment, and new infections arise both through exposure to contaminated water, as well as by the classical SIR person–person transmission pathway. We compute the basic reproductive number ($\mathcal{R}_0$), epidemic growth rate, and final outbreak size for the resulting "SIWR" model, and examine how these fundamental quantities depend upon the transmission parameters for the different pathways. We prove that the endemic disease equilibrium for the SIWR model is globally stable. We identify the pathogen decay rate in the water compartment as a key parameter determining when the distinction between the different transmission routes in the SIWR model is important. When the decay rate is slow, using an SIR model rather than the SIWR model can lead to under-estimates of the basic reproductive number and over-estimates of the infectious period.

Keywords Waterborne pathogens · Disease transmission routes

1. Introduction

Waterborne disease studies have a celebrated place in epidemiology and public health, with John Snow's investigations on London cholera outbreaks in the 1800s being a crucial step in establishing the germ theory of disease (Snow, 1936). Unfortunately, waterborne diseases remain a serious public health concern today, resulting in more than 3.5 million deaths a year according to WHO estimates (Prüss-Üstün et al., 2008). Severe waterborne disease outbreaks continue to occur, such as the Zimbabwe cholera epidemic from August 2008 to July 2009 which caused more than 98,000 cases and 4,200 deaths (WHO, 2009).

*Corresponding author.
E-mail address: jtien@math.ohio-state.edu (Joseph H. Tien).

Several different factors must be considered in attempting to understand waterborne disease dynamics, including sanitation and different transmission pathways (Ashbolt, 2004; Eisenberg et al., 2002; Hunter et al., 2003), water treatment efforts (Ashbolt, 2004), pathogen ecology outside of human hosts (e.g. Faruque et al., 1998; Rose, 1997), and climatological factors such as El Niño (Pascual et al., 2000) or rainfall (Auld et al., 2004; Curriero et al., 2001). Unraveling how these factors interact to shape disease dynamics is challenging. The objective of the work presented here is to deepen our understanding of how different transmission pathways affect disease dynamics by extending classical mathematical epidemic theory to SIR-type models that include a water compartment.

There is some ambiguity as to what constitutes a waterborne disease (Ashbolt, 2004). For the purposes of this paper, we consider a waterborne disease to be any disease for which transmission through water is a concern. A small sampling of diseases in this category includes cholera, *Giardia*, *Cryptosporidium*, *Campylobacter*, hepatitis A and E, norovirus, rotavirus, and *E. coli* O157:H7 (Ashbolt, 2004; Butzler, 2004; Ford, 1999; Gerba et al., 1996; Karanis et al., 2007; Leclerc et al., 2002; Marshall et al., 1997; Sack et al., 2004; Schuster et al., 2005). Infection for each of these diseases is typically through pathogen ingestion (e.g. fecal–oral route). However, many different specific transmission pathways are possible, such as drinking sewage-contaminated water, eating food prepared by an individual with soiled hands, or acquiring an infection during treatment in a hospital. The relative contribution of the different transmission pathways may vary not only between diseases, but also between outbreaks for a given disease. For example, cholera transmission is typically thought to occur by drinking contaminated water, but an outbreak in a Singapore psychiatric hospital appears to have been driven by direct person–person transmission (Goh et al., 1990). *Giardia* is frequently contracted by drinking contaminated water, but direct contact with infected individuals is also an established risk factor (Andersen and Neumann, 2007). On the other hand, hepatitis A transmission occurs primarily through person–person contact, with contaminated water providing a secondary transmission route (Nasser, 1994).

A number of different approaches have been used for modeling waterborne disease transmission. Eisenberg et al. (2003) formulate a stochastic model where infected individuals create secondary infections both within a household through direct person–person contact, and between households by shedding pathogen into a common water source. King et al. (2008) present stochastic differential equation models of cholera that include both person-person transmission, and transmission from an environmental reservoir ("water–person" transmission), but with no feedback from infected individuals into the environmental reservoir. Several studies present compartmental ODE models where infections arise solely by "person–water–person" transmission, where infected individuals shed pathogen into a water source from which susceptible individuals then drink (Codeco, 2001; Faruque et al., 2005; Hartley et al., 2006). These models exclude person–person transmission. The standard SIR/SIRS framework has also been used to model waterborne diseases (Koelle et al., 2005, 2006).

Here, we consider a simple extension of the classical SIR model by adding a water compartment W, and allowing for both person–person and person–water–person transmission. We derive fundamental quantities for the resulting "SIWR model", such as the basic reproductive number, epidemic growth rate, and final outbreak size, and examine how these quantities depend upon the transmission parameters for the different pathways. We identify the time scale for pathogen dynamics in the water compartment as a key

parameter determining when the two transmission pathways can be well approximated by a single pathway, and consider potential pitfalls of neglecting person–water–person transmission when pathogen dynamics in the water are slow.

The remainder of this paper is organized as follows. Section 2 presents the SIWR model equations. Analytical results for the model are given in Section 3. Section 4 compares the SIWR and SIR models both numerically, and through a fast-slow analysis of the SIWR model. We conclude with a discussion in Section 5.

2. SIWR model equations

Figure 1 shows the flow diagram for the basic model we will analyze. A very similar flow diagram was presented in Eisenberg et al. (2002), and analyzed as a Markov chain model in Eisenberg et al. (2003). The treatment in this paper will be as a compartmental ODE model, similar to the classic SIR framework. The model consists of the standard SIR model under the assumption of constant population size (Anderson and May, 1991), together with a compartment W that measures pathogen concentration in a water source. Susceptible individuals become infected either by contact with infected individuals or through contact with contaminated water. Infected individuals can in turn contaminate the water compartment by shedding the pathogen into W. An infected individual thus generates secondary infections in two ways: through direct contact with susceptible individuals, and by first shedding the pathogen into the water compartment, which susceptible individuals subsequently come into contact with. The corresponding model equations are

$$\begin{aligned} \dot{S} &= \mu N - b_W W S - b_I S I - \mu S, \\ \dot{I} &= b_W W S + b_I S I - \gamma I - \mu I, \\ \dot{W} &= \alpha I - \xi W, \\ \dot{R} &= \gamma I - \mu R. \end{aligned} \tag{1}$$

As in the SIR model, the $\dot{R}$ equation can be eliminated from the system.

Parameters b_W, b_I are the transmission rate parameters for water-to-person and person-to-person contact, respectively. The birth and non-disease-related death rate is given by μ. The mean infectious period is given by $1/\gamma$. The pathogen shedding rate from infected individuals into the water compartment is given by α, and ξ gives the decay rate of pathogen in the water. Tables 1 and 2 summarize the model variables and parameters.

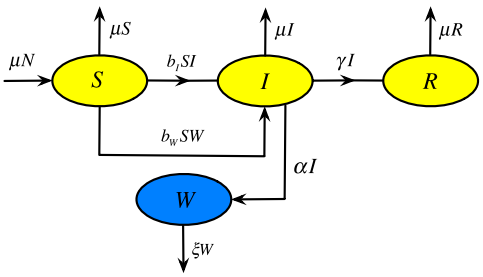

Fig. 1 Flow diagram for the SIWR model (1). See Tables 1–2.

Table 1 Variables for the SIWR model (1), together with sample units

S	susceptible individual density	individuals km^{-2}
I	infected individual density	individuals km^{-2}
R	recovered/removed individual density	individuals km^{-2}
W	pathogen concentration in water reservoir	cells ml^{-3}
N	total population density	individuals km^{-2}

Table 2 Parameters for the SIWR models (1) and (2), together with sample units

b_I	person–person contact rate	km^2 individuals^{-1} day^{-1}
β_I	scaled person–person contact rate	day^{-1}
b_W	reservoir–person contact rate	ml^3 cells^{-1} day^{-1}
β_W	scaled reservoir–person contact rate	day^{-1}
μ	birth/death rate	day^{-1}
$1/\gamma$	infectious period	day
$1/\xi$	pathogen lifetime in water reservoir	day
α	person–reservoir contact rate ("shedding")	cells ml^{-3} day^{-1} km^2 individuals^{-1}

It is instructive to consider a rescaling of system (1) that gives dimensionless variables. Let N denote the total population size, and let $s = S/N, i = I/N, r = R/N, w = \frac{\xi}{\alpha N} W$. This gives the following rescaled system:

$$\begin{aligned} \dot{s} &= \mu - \beta_W w s - \beta_I s i - \mu s, \\ \dot{i} &= \beta_W w s + \beta_I s i - \gamma i - \mu i, \\ \dot{w} &= \xi(i - w), \\ \dot{r} &= \gamma i - \mu r. \end{aligned} \tag{2}$$

The transmission rate parameters b_W, b_I in system (1) are replaced by $\beta_W = b_W N \alpha/\xi$, $\beta_I = b_I N$ in system (2). Note that β_W reflects both water-to-person transmission (b_W), as well as person-to-water shedding (α). We will refer to β_W as the transmission parameter for the person–water–person transmission route. The phase space for system (2) is

$$\Omega = \{s, i, w, r \geq 0 : s + i + r = 1\}. \tag{3}$$

We will focus primarily on the scaled system (2) in this paper. We include the scaled SIR model equations below for reference:

$$\begin{aligned} \dot{s} &= \mu - \beta s i - \mu s, \\ \dot{i} &= \beta s i - \gamma i - \mu i, \\ \dot{r} &= \gamma i - \mu r. \end{aligned} \tag{4}$$

Note that the (s, i, r) subsystem of (2) reduces to the SIR system (4) when $\beta_W = 0$.

System (2) is a very simple extension of the SIR framework. No latent period is included, and the infectious period and pathogen lifetime in the water compartment are both modeled as being exponentially distributed. Multiple infected compartments are commonly used to model diseases with latent period, different stages of disease progression (Hyman and Li, 1999; Wagner and Earn, 2010), and gamma distributed latent and infectious periods (Anderson and Watson, 1980). An extension of (2) that includes multiple

infected compartments is given in the Appendix. However, our analysis will focus on system (2).

3. Model analysis

We first establish some preliminary facts concerning the long term behavior of solutions to system (2). For any $\epsilon > 0$, we define

$$\Omega_{w\leq 1+\epsilon} = \{(s, i, w, r) \in \Omega : w \leq 1 + \epsilon\}. \tag{5}$$

The following lemma shows that solutions to system (2) exist for all $t > 0$ and eventually lie in $\Omega_{w\leq 1+\epsilon}$.

Lemma 1. *Let $\epsilon > 0$ and define Ω and $\Omega_{w\leq 1+\epsilon}$ with (3) and (5), respectively. Let $x(t)$ denote the solution to system (2) with initial condition $x(0) \in \Omega$. Then $x(t) \in \Omega$ for all $t > 0$. Furthermore, there exists $T_\epsilon > 0$ such that for all $t > T_\epsilon$, $x(t) \in \Omega_{w\leq 1+\epsilon}$.*

Proof: To see that solutions to system (2) starting from any point in Ω remain in Ω, let $n = s + i + r$. Then $\dot{n} = \mu - \mu n$, so $n = 1$ is a fixed point. As $n(0) = 1$, we have $s(t) + i(t) + r(t) = 1$. Next, consider (2) when at least one of the phase space variables x_i is equal to 0. Direct computation gives that if $x_i = 0$, then $\dot{x}_i \geq 0$. Thus, solutions trajectories to (2) do not leave through the boundary of Ω in forward time.

As $i \leq 1$, from the $\dot{w}$ equation in (2), we have that $\dot{w} < 0$ when $w > 1$. Hence, $w(t)$ is decreasing for any $w > 1$, giving that $w(t)$ (and hence $x(t)$) is bounded. Solutions to (2) with initial condition in Ω thus exist for all $t > 0$ (Hirsch and Smale, 1974, p. 171). Finally, to see that $x(t)$ is eventually contained in $\Omega_{w\leq 1+\epsilon}$, note that $\dot{w} < 0$ for $w = 1 + \epsilon$, giving that solutions which have entered $\Omega_{w\leq 1+\epsilon}$ remain in $\Omega_{w\leq 1+\epsilon}$. So, it remains to show that solutions starting from $w_0 > 1 + \epsilon$ enter $\Omega_{w\leq 1+\epsilon}$. Whenever $w > 1 + \epsilon$, $\dot{w} < -\xi\epsilon$, so with $w_0 > 1 + \epsilon$ we have $w(t) < w_0 - \xi\epsilon t$ as long as w remains greater than $1 + \epsilon$. Now define $T_\epsilon = [w_0 - (1 + \epsilon)]/\xi\epsilon$. If the solution is still outside $\Omega_{w\leq 1+\epsilon}$ at time T_ϵ, then $w(T_\epsilon) < w_0 - \xi\epsilon T_\epsilon = 1 + \epsilon$, a contradiction. Hence, the solution must enter $\Omega_{w\leq 1+\epsilon}$ before time T_ϵ. □

3.1. Basic reproductive number and equilibria

The basic reproductive number $\mathcal{R}_0$ is defined as the expected number of secondary infections that result from introducing a single infected individual into an otherwise susceptible population. $\mathcal{R}_0$ is a fundamental quantity in mathematical epidemiology, which—in the deterministic limit—dictates whether a newly invading pathogen will cause a disease outbreak (Anderson and May, 1991). Here, we use a second generation matrix approach to compute the basic reproductive number (van den Driessche and Watmough, 2002).

As in van den Driessche and Watmough (2002), we write the second generation matrix at the disease free equilibrium as FV^{-1}, where the ij entry of the matrix F is the rate at which infected individuals in compartment j produce new infections in compartment i,

and the jk entry of V^{-1} is the average duration of stay in compartment j starting from k. For system (2), we have

$$F = \begin{pmatrix} \beta_I & \beta_W \\ 0 & 0 \end{pmatrix}, \tag{6a}$$

$$V^{-1} = \begin{pmatrix} \frac{1}{\gamma+\mu} & 0 \\ \frac{1}{\gamma+\mu} & \frac{1}{\xi} \end{pmatrix}. \tag{6b}$$

The basic reproductive number corresponds to the spectral radius of FV^{-1},

$$\begin{aligned} \mathcal{R}_0 &= \rho\left(FV^{-1}\right) \\ &= \frac{\beta_I + \beta_W}{\gamma + \mu}. \end{aligned} \tag{7}$$

System (2) possesses a "disease-free" equilibrium at $(s, i, w) = (1, 0, 0)$. For $\mathcal{R}_0 > 1$ and $\mu > 0$, system (2) also has an "endemic" equilibrium $x^* = (s^*, i^*, w^*)$, where

$$(s^*, i^*, w^*) = \left(\frac{1}{\mathcal{R}_0}, \frac{\mu}{\gamma + \mu}(1 - s^*), i^*\right). \tag{8}$$

3.2. Epidemic growth rate

It is a general result that the local stability of the disease-free equilibrium is determined by $\mathcal{R}_0$, with stability for $\mathcal{R}_0 < 1$ and instability when $\mathcal{R}_0 > 1$ (e.g. Theorem 2 in van den Driessche and Watmough, 2002). When $\mathcal{R}_0 > 1$, a disease outbreak occurs (in deterministic systems). The dominant eigenvalue of the Jacobian at the disease free equilibrium is typically referred to as the initial outbreak growth rate. Below we compute the initial outbreak growth rate for system (2). This will allow us to examine how varying the contributions of the different transmission pathways affects the growth rate, and gives useful results for estimating $\mathcal{R}_0$ from an empirically observed growth rate.

Let λ denote the initial outbreak growth rate for system (2). When $\mathcal{R}_0 > 1$, calculating the dominant eigenvalue of the Jacobian at the disease-free equilibrium for system (2) gives

$$\begin{aligned} \lambda &= \frac{\beta_I - \mu - \gamma - \xi + \sqrt{(\beta_I - \mu - \gamma + \xi)^2 + 4\xi\beta_W}}{2} \\ &= \frac{\tilde{\lambda} - \xi + \sqrt{(\tilde{\lambda} + \xi)^2 + 4\xi\beta_W}}{2}, \end{aligned} \tag{9}$$

where

$$\tilde{\lambda} = \beta_I - (\gamma + \mu). \tag{10}$$

Note that $\tilde{\lambda}$ has the same form as the growth rate for a disease outbreak in the classical SIR model (Anderson and May, 1991). When an outbreak occurs in the limit of no transmission from the water ($\beta_W \to 0$), system (2) collapses to an SIR model and $\lambda \to \tilde{\lambda}$. In

addition, since it will be useful later, we note from (9) that

$$\lambda \geq \tilde{\lambda}. \tag{11}$$

Estimating the basic reproductive number from time series data is often of interest. Wallinga and Lipsitch (2007) discuss how empirically observed growth rates can be combined with knowledge of the distribution of disease generation times to estimate $\mathcal{R}_0$. In system (2), the generation time is affected by both the mean infectious period and the pathogen lifetime in the water compartment. Let $T_I = 1/(\gamma + \mu)$ denote the mean time spent in the infectious class, and let $T_W = 1/\xi$ denote the mean pathogen lifetime in the water compartment. After some algebra, Eq. (9) can be rearranged to give the following expression linking $\mathcal{R}_0$ and λ:

$$\mathcal{R}_0^{\text{siwr}} = 1 + T_I\lambda\big(1 + T_W(\lambda - \tilde{\lambda})\big). \tag{12}$$

Note that (12) involves both T_I and T_W. In the limit of no water transmission (in which case $\lambda = \tilde{\lambda}$ as noted above), Eq. (12) reduces to the relationship between the basic reproductive number and growth rate for the SIR model (4):

$$\mathcal{R}_0^{\text{sir}} = 1 + T_I\lambda_{\text{sir}}, \tag{13}$$

where $\lambda_{\text{sir}} = \beta - (\gamma + \mu)$.

To illustrate how the water compartment affects $\mathcal{R}_0$ estimates, we compare SIR and SIWR $\mathcal{R}_0$ estimates for the same data set. Suppose that an observed growth rate λ_{obs} is available, for example from incidence time series data. Let parameters be chosen for the SIR (4) and SIWR (2) systems so that the growth rates for each model match the observed growth rate λ_{obs}. Then the following proposition shows that when the mean infectious period $(1/\gamma)$ and birth rate (μ) are known, the SIWR $\mathcal{R}_0$ value is greater than or equal to the $\mathcal{R}_0$ value in the SIR model.

Proposition 1. *Let $\lambda_{\text{obs}} > 0$ be fixed. Consider parameters for the SIR (4) and SIWR (2) systems, such that the growth rates in both models are equal to λ_{obs}. Let $T_I = 1/(\gamma + \mu)$ be the same for both models. Let $\hat{\mathcal{R}}_0^{\text{sir}}$, $\hat{\mathcal{R}}_0^{\text{siwr}}$ denote the corresponding values for $\mathcal{R}_0$ in systems (4) and (2), respectively. Then $\hat{\mathcal{R}}_0^{\text{siwr}} \geq \hat{\mathcal{R}}_0^{\text{sir}}$.*

Proof: From (12), we have $\hat{\mathcal{R}}_0^{\text{siwr}} = 1 + T_I\lambda_{\text{obs}}(1 + T_W(\lambda_{\text{obs}} - \tilde{\lambda}))$. From (13), we have $\hat{\mathcal{R}}_0^{\text{sir}} = 1 + T_I\lambda_{\text{obs}}$. Subtracting these two expressions gives

$$\begin{aligned}\hat{\mathcal{R}}_0^{\text{siwr}} - \hat{\mathcal{R}}_0^{\text{sir}} &= T_I T_W \lambda_{\text{obs}}(\lambda_{\text{obs}} - \tilde{\lambda}) \\ &= T_I T_W \lambda(\lambda - \tilde{\lambda}),\end{aligned} \tag{14}$$

as the growth rate λ of the SIWR model (2) matches the observed growth rate λ_{obs} by assumption. Noting that $\lambda - \tilde{\lambda} \geq 0$ [cf. (11)] gives that $\hat{\mathcal{R}}_0^{\text{siwr}} - \hat{\mathcal{R}}_0^{\text{sir}} \geq 0$ as claimed. □

From a practical standpoint, Proposition 1 states that if the mean infectious period is known then neglecting the water compartment and fitting an SIR model to an observed growth rate results in an underestimate of the reproductive number.

Growth rate for fixed $\mathcal{R}_0$ One way to examine the effect of varying the relative contributions of the person–person and person–water–person transmission pathways on disease dynamics is to vary β_I and β_W under the constraint that $\mathcal{R}_0$ be kept fixed. The following proposition shows that increasing the relative contribution of person–water–person transmission for fixed $\mathcal{R}_0 > 1$ results in a slower epidemic growth rate.

Proposition 2. *Let $\mathcal{R}_0 > 1$ be held fixed for system (2). Let the growth rate of the epidemic, λ, be given by Eq. (9), and let $\frac{d\lambda}{d\beta_W}$ denote the total derivative of λ with respect to β_W. Then $\frac{d\lambda}{d\beta_W} < 0$.*

Proof: The growth rate λ depends upon both β_I and β_W. Under the assumption of fixed $\mathcal{R}_0$, β_I is determined by β_W through the constraint $\beta_I = \mathcal{R}_0(\gamma + \mu) - \beta_W$. The basic reproductive number $\mathcal{R}_0$ for system (2) is given by Eq. (12), which involves the term $\tilde{\lambda} = \beta_I - (\gamma + \mu)$ [cf. (10)]. We will need the total derivative of $\tilde{\lambda}$:

$$\begin{aligned}\frac{d}{d\beta_W}\tilde{\lambda}(\beta_I(\beta_W), \beta_W) &= \frac{\partial\tilde{\lambda}}{\partial\beta_I}\frac{\partial\beta_I}{\partial\beta_W} + \frac{\partial\tilde{\lambda}}{\partial\beta_W} \\ &= -1. \end{aligned} \tag{15}$$

Taking the total derivative of both sides of (12) with respect to β_W, recalling that $\mathcal{R}_0$ is fixed and using (15), we have

$$0 = T_I T_W \left[\frac{d\lambda}{d\beta_W}(\lambda - \tilde{\lambda} + \xi) + \lambda\left(\frac{d\lambda}{d\beta_W} + 1\right)\right], \tag{16}$$

where $T_I = 1/(\gamma + \mu)$ and $T_W = 1/\xi$. Solving for $\frac{d\lambda}{d\beta_W}$ gives

$$\frac{d\lambda}{d\beta_W} = \lambda/\big[(\tilde{\lambda} - \lambda) - (\xi + \lambda)\big]. \tag{17}$$

As $\mathcal{R}_0 > 1$, $\lambda > 0$. We also have $\tilde{\lambda} \le \lambda$ [cf. (11)]. Finally, $\xi > 0$ on physical grounds. Thus, the numerator is positive and the denominator negative in (17), giving that $\frac{d\lambda}{d\beta_W} < 0$. □

It is instructive to consider the relationship between $\frac{d\lambda}{d\beta_W}$ (the total derivative of the growth rate with respect to β_W when $\mathcal{R}_0 > 1$ is fixed) and the partial derivatives of λ with respect to β_I, β_W:

$$\frac{d\lambda}{d\beta_W} = -\frac{\partial\lambda}{\partial\beta_I} + \frac{\partial\lambda}{\partial\beta_W}. \tag{18}$$

The growth rate is an increasing function of both β_I and β_W. Together with Proposition 2, Eq. (18) shows that the growth rate is more sensitive to person–person transmission than to person–water–person transmission.

Corollary 1. *Let the initial epidemic growth rate λ be given by (9), and let $\mathcal{R}_0 > 1$. Then $\frac{\partial\lambda}{\partial\beta_I} > \frac{\partial\lambda}{\partial\beta_W}$.*

Proof: From Proposition 2, we have $\frac{d\lambda}{d\beta_W} < 0$. From (18), $\frac{d\lambda}{d\beta_W} = -\frac{\partial\lambda}{\partial\beta_I} + \frac{\partial\lambda}{\partial\beta_W}$, giving that $\frac{\partial\lambda}{\partial\beta_I} > \frac{\partial\lambda}{\partial\beta_W}$. □

Bounds for estimating $\mathcal{R}_0$ from an outbreak growth rate A difficulty in estimating $\mathcal{R}_0$ from an observed outbreak growth rate is that the relationship between $\mathcal{R}_0$ and λ involves both person–person (β_I) and person–water–person (β_W) transmission [cf. (12)]. If we cannot estimate the transmission parameters associated with each transmission route separately, then the basic reproductive number is not uniquely determined by the observed epidemic growth rate. In this situation, a range of transmission parameter values β_I, β_W can result in the same specified growth rate, but different $\mathcal{R}_0$ values. We can, however, derive bounds for the possible $\mathcal{R}_0$ values.

Consider Eq. (12). Let parameters of system (2) be chosen so that λ matches an observed growth rate λ_{obs}. Proposition 1 gives that $\mathcal{R}_0$ is minimized when the SIWR model reduces to an SIR model. Hence, a lower bound for $\mathcal{R}_0$ is $1 + T_I\lambda$, the reproductive number for an SIR model. The term $\tilde{\lambda} = \beta_I - (\gamma + \mu)$ increases with β_I. For fixed $\lambda = \lambda_{\text{obs}}$, we then have that $\mathcal{R}_0$ is a decreasing function of β_I. As $\beta_I \geq 0$, we have that $\mathcal{R}_0$ is maximized when $\beta_I = 0$. This gives the following bounds for $\mathcal{R}_0$ (which do not depend on the unobservable transmission rates β_I and β_W):

$$1 + T_I\lambda_{\text{obs}} \leq \mathcal{R}_0 \leq 1 + T_I T_W \lambda_{\text{obs}}(\lambda_{\text{obs}} + \gamma + \mu + \xi). \tag{19}$$

3.3. Stability of the endemic equilibrium

An endemic equilibrium exists for system (2) when $\mathcal{R}_0 > 1$. In this section, we analyze the stability of the endemic equilibrium.

Local stability Consider the Jacobian at the endemic equilibrium:

$$J|_{x^*} = \begin{pmatrix} -\frac{\mu}{s^*} & -\beta_I s^* & -\beta_W s^* \\ \mu(\frac{1}{s^*} - 1) & \beta_I s^* - (\gamma + \mu) & \beta_W s^* \\ 0 & \xi & -\xi \end{pmatrix}. \tag{20}$$

The characteristic polynomial is $\lambda^3 + a_1\lambda^2 + a_2\lambda + a_3$, where

$$\begin{aligned} a_1 &= \xi + \beta_W s^* + \tfrac{\mu}{s^*}, \\ a_2 &= \mu\left[\beta_I(1 - s^*) + \frac{\xi}{s^*} + \beta_W\right], \\ a_3 &= \xi\mu(1 - s^*)(\beta_I + \beta_W). \end{aligned} \tag{21}$$

Since $\mathcal{R}_0 > 1$ and $s^* = 1/\mathcal{R}_0$, we have $1 - s^* > 0$, so $a_i > 0$ for $i = 1, 2, 3$. The Routh–Hurwitz criteria give that the endemic equilibrium is stable if $a_1 > 0, a_3 > 0$, and $a_1 a_2 > a_3$. Thus, local stability of the endemic equilibrium is determined by the sign of $a_1 a_2 - a_3$. This turns out to be always positive:

$$\begin{aligned} a_1 a_2 - a_3 &= \frac{\xi^2\mu}{s^*} + \xi\mu\beta_W s^* + \left(\beta_W s^* + \frac{\mu}{s^*}\right)\mu\left[\beta_I(1 - s^*) + \frac{\xi}{s^*} + \beta_W\right] \\ &> 0. \end{aligned} \tag{22}$$

Thus, the endemic equilibrium in system (2) is locally stable whenever it exists.

Global stability We now show that whenever it exists the endemic equilibrium for system (2) is globally stable. We do this by finding a Lyapunov function of the general form considered by Korobeinikov and Wake (2002) and Korobeinikov (2004) for the SIR and SEIR models.

Let Ω denote the phase space (3), and let Ω_D denote the subset of Ω where disease is present, i.e.

$$\Omega_D = \big\{(s, i, w) \in \Omega : (i, w) \neq (0, 0)\big\}. \tag{23}$$

We wish to show that when $\mathcal{R}_0 > 1$, $x(t) \to x^*$ for any initial condition in Ω_D. We do this by finding a Lyapunov function on the interior of Ω, and then showing that trajectories starting in Ω_D enter the interior of Ω.

Let $\operatorname{int}\Omega = \{(s, i, w) \in \Omega : s \neq 0, i \neq 0, w \neq 0\}$ and let $V : \operatorname{int}\Omega \to \mathbb{R}$ be defined as:

$$V(s, i, w) = s - s^* \log s + i - i^* \log i + \frac{\beta_W}{\beta_I + \beta_W} \frac{\gamma + \mu}{\xi} (w - w^* \log w). \tag{24}$$

Note that V is continuous on $\operatorname{int}\Omega$, and has a global minimum at $x^* = (s^*, i^*, w^*)$.

The time derivative of V is

$$\begin{aligned}
\dot{V} &= 2\mu - \mu s - \mu \frac{s^*}{s} \\
&\quad - \beta_W s^* i^* \left(\frac{i}{w} - 1 \right) - \beta_W s i^* \frac{w}{i} - \beta_I s i^* \\
&= -\mu \left(\frac{s^*}{s} + \frac{s}{s^*} - 2 \right) \\
&\quad - \beta_W s^* i^* \left[\frac{i}{w} - 1 + \frac{s}{s^*} \left(\frac{w}{i} - 1 \right) \right] \\
&= (\beta_W s^* i^* - \mu) \left(\frac{s}{s^*} + \frac{s^*}{s} - 2 \right) \\
&\quad - \beta_W s^* i^* \left(\frac{i}{w} + \frac{s}{s^*} \frac{w}{i} + \frac{s^*}{s} - 3 \right).
\end{aligned} \tag{25}$$

To show that $\dot{V} \leq 0$, we use the fact that the geometric mean is less than or equal to the arithmetic mean. This is the key to the Lyapunov functions of the form $\sum C_j (x_j - x_j^* \log x_j)$ considered by Korobeinikov and Wake (2002) and Korobeinikov (2004). We have

$$\begin{aligned}
1 &= \sqrt{\frac{s^*}{s} \frac{s}{s^*}} \\
&\leq \frac{1}{2} \left(\frac{s^*}{s} + \frac{s}{s^*} \right),
\end{aligned}$$

giving $\frac{s^*}{s} + \frac{s}{s^*} - 2 \geq 0$. Similarly, we have that $\frac{i}{w} + \frac{s}{s^*} \frac{w}{i} + \frac{s^*}{s} - 3 \geq 0$. Thus, examining (25), we see that to show that $\dot{V} \leq 0$, it suffices to establish that $\beta_W s^* i^* - \mu < 0$.

Using the expression for i^* in (8), we have

$$\begin{aligned}\beta_W s^* i^* - \mu &= \mu\left[\frac{\beta_W}{\gamma+\mu}s^*(1-s^*)-1\right]\\ &\le \mu\left[\frac{\beta_W+\beta_I}{\gamma+\mu}s^*(1-s^*)-1\right]\\ &= \mu\left[\frac{1}{s^*}s^*(1-s^*)-1\right]\\ &= -\mu s^*\\ &< 0, \end{aligned} \tag{26}$$

giving $\dot{V} \le 0$.

Proposition 3. *Let the sets Ω, Ω_D and $\operatorname{int}\Omega$ and the function $V : \operatorname{int}\Omega \to \mathbb{R}$ be defined as above. Let $\mu > 0$ and the basic reproductive number $\mathcal{R}_0 > 1$ in system (2), and let x^* denote the endemic equilibrium given in (8). Then every solution trajectory of (2) with initial condition in Ω_D converges to x^* as $t \to \infty$.*

Proof: First note that solutions starting from $\Omega_D - \operatorname{int}\Omega$ enter $\operatorname{int}\Omega$. In $\Omega_D - \operatorname{int}\Omega$, we either have $s = 0$, or $s \neq 0$ and exactly one of i or w is zero. As $\dot{s} = \mu > 0$ when $s = 0$, it is sufficient to consider the $s \neq 0$ case. In the situation where $i = 0$ and $w > 0$, we have $\dot{i} = \beta_W w s > 0$. In the case where $i > 0$ and $w = 0$, we have $\dot{w} = \xi i > 0$. In both cases, the tangent vectors point into $\operatorname{int}\Omega$, and thus $x(t)$ enters $\operatorname{int}\Omega$.

From (25), we have $\dot{V} \le 0$ on $\operatorname{int}\Omega$. Let L denote the set of points where $\dot{V}$ is zero. As $t \to \infty$, $x(t)$ approaches the largest invariant set in L (cf. Theorem VIII in LaSalle and Lefschetz (1961)). By Lemma 1, this invariant set is contained in $\Omega_{w \le 1+\epsilon} \subset \Omega$. It remains to show that the fixed point $\{x^*\}$ is the only invariant set in L. There are two cases to consider: $\beta_W = 0$, and $\beta_W > 0$.

When $\beta_W > 0$, $L = \{s = s^*, w = i\}$. Let x belong to an invariant set contained in L. We have $s(t) = s^*$ and $w(t) = i(t)$ along solution trajectories to (2) in this invariant set. Setting $\dot{s} = 0$ with $s = s^*$ and $w = i$ gives

$$\mu - (\beta_I + \beta_W)s^* i - \mu s^* = 0.$$

Solving for i, we have

$$i = \frac{\mu(1-s^*)}{(\beta_I+\beta_W)s^*} = i^*.$$

As $w = i$ in L, we have $w = i^* = w^*$. Thus, the largest invariant set in L is $\{x^*\}$.

Finally, in the $\beta_W = 0$ case, $L = \{s = s^*\}$. Trajectories $x(t)$ belonging to an invariant set in L have $s(t) = s^*$. Setting $\dot{s} = 0$ with $s = s^*$ and solving for i gives

$$\begin{aligned} i &= \mu(1-s^*)/\beta_I s^*\\ &= \frac{\mu}{\gamma+\mu}(1-s^*)\\ &= i^*. \end{aligned}$$

Both s and i are thus constant within invariant sets in L, leaving w as the remaining one-dimensional system to consider. From the $\dot{w}$ equation in (2), we have that $w(t)$ is increasing for $w < i^*$, and decreasing for $w > i^*$. Invariance is thus possible only when $w = w^*$, giving that the largest invariant set in L consists of x^* alone. □

3.4. Final outbreak size

In the absence of births and deaths ($\mu = 0$), disease outbreaks in system (2) eventually "burn out" due to depletion of the susceptible pool. In this section, we consider Z, the proportion of the population that is eventually infected by a newly invading pathogen with $\mathcal{R}_0 > 1$. A classic result from mathematical epidemiology is the final outbreak size relation for the SIR model:

$$Z = 1 - \exp(-\mathcal{R}_0 Z). \tag{27}$$

This relation for the final outbreak size is also valid for many extensions of the basic SIR model (Kermack and McKendrick, 1927; Ma and Earn, 2006). We show here that the final outbreak size relation holds for the SIWR system (2) as well, using the same approach as Ma and Earn's proof of (27) for staged-progression models (Ma and Earn, 2006). We first establish that in the absence of births and deaths, disease outbreaks eventually "burn out".

Lemma 2. *Let $\mathcal{R}_0 > 1$ and $\mu = 0$ in system (2). Then $i(t) \to 0$ and $w(t) \to 0$ as $t \to \infty$.*

Proof: Let Γ_+ denote the ω-limit set of the solution trajectory to (2) with initial condition $x_0 \in \Omega$. For $\mu = 0$, $\dot{s} \leq 0$. Hence, $s(t)$ is decreasing and bounded below, so $s(t)$ converges to a limit $\bar{s}$. The s component of any point in Γ_+ is thus equal to $\bar{s}$.

By Lemma 1, for any $\epsilon > 0$ Γ_+ is contained within the compact set $\Omega_{w \leq 1+\epsilon} \subset \Omega$ [cf. (5)]. So, take any point $\bar{x} \in \Gamma_+$, and consider solution trajectories to (2) starting from $\bar{x}$. As Γ_+ is invariant (Guckenheimer and Holmes, 1983), $s(t) = \bar{s}$ along solution trajectories in Γ_+, and thus $\dot{s} = 0$ within Γ_+. From the $\dot{s}$ equation in (2), we either have $(i, w) = (0, 0)$, or $\bar{s} = 0$. If $(i, w) = (0, 0)$ we are done, so consider the case where $\bar{s} = 0$. Fixing $\bar{s} = 0$ in (2) gives a linear system for (i, w) with eigenvalues $-\gamma, -\xi$. The only invariant set for this linear system is the origin, giving that the ω-limit set consists of the point $(\bar{s}, 0, 0)$. □

We now prove that the final outbreak size relation holds for newly invading pathogens in system (2) with $\mathcal{R}_0 > 1$ and $\mu = 0$.

Proposition 4. *Let $\mu = 0$ and $\mathcal{R}_0 > 1$ for system (2). Let s_0 denote the initial susceptible proportion, and w_0 the initial pathogen level in the water. In the limits $s_0 \to 1$ and $w_0 \to 0$, the total proportion of the population infected over the course of an outbreak in system (2) approaches the solution Z to the final outbreak size relation (27).*

Proof: Let

$$F(t) = \log s(t) + \frac{\beta_I + \beta_W}{\gamma} r(t) - \frac{\beta_W}{\xi} w(t).$$

Then $F(t)$ is a constant along solution trajectories of system (2). The removed proportion $r(t)$ increases monotonically to a limit $\bar{r}$, and $s(t)$ decreases monotonically to $\bar{s}$. By Lemma 2, $i(t) \to 0$. As $s(t) + i(t) + r(t) = 1$, we have that $\bar{s} = 1 - \bar{r}$. Lemma 2 also gives that $w(t) \to 0$, yielding

$$\lim_{t\to\infty} F(t) = \log(1-\bar{r}) + \frac{\beta_I + \beta_W}{\gamma}\bar{r}.$$

On the other hand, at $t = 0$, we have

$$F(0) = \log s_0 + \frac{\beta_I + \beta_W}{\gamma} r_0 - \frac{\beta_W}{\xi} w_0.$$

As F is constant along solution trajectories, we have $\lim_{t\to\infty} F(t) = F(0)$:

$$\log(1-\bar{r}) + \frac{\beta_I + \beta_W}{\gamma}(\bar{r} - r_0) + \frac{\beta_W}{\xi} w_0 = \log s_0.$$

Letting $s_0 \to 1$, $w_0 \to 0$ in the resulting expression, and noting that $s_0 \to 1$ forces $i_0 \to 0$ and $r_0 \to 0$, gives

$$\log(1-\bar{r}) + \frac{\beta_I + \beta_W}{\gamma}\bar{r} = 0.$$

Finally, noting that $\bar{r} \to Z$ as $r_0 \to 0$, and that $\mathcal{R}_0 = \frac{\beta_I+\beta_W}{\gamma}$ when $\mu = 0$, gives the desired result. □

The final outbreak size relation also holds for the extension of the SIWR model to include multiple infected compartments. This is demonstrated in the Appendix.

An interesting feature of system (2) is that a newly invading pathogen can take the form of a sudden pathogen influx in the water, for example through the failure of a water treatment plant. In this situation, w_0 and s_0 may both be large. The proof of Proposition 4 also gives the relationship between the final outbreak size and the initial amount of pathogen in the water for this situation.

Remark 1. Let $\mu = 0$ and $\mathcal{R}_0 > 1$ for system (2). Let s_0 denote the initial susceptible proportion, and w_0 the initial pathogen level in the water. In the limit $s_0 \to 1$, the final outbreak size Z satisfies the relation

$$Z = 1 - \exp\left(-\mathcal{R}_0 Z - \frac{\beta_W}{\xi} w_0\right). \tag{28}$$

4. Comparison of SIR and SIWR dynamics

The person–person (β_I) and person–water–person (β_W) transmission rates are key parameters in the SIWR system (2). The basic reproductive number and initial outbreak growth rate depend upon β_I and β_W (cf. Section 3), and outbreaks with different (β_I, β_W) values may require different intervention strategies. Methods for estimating the extent of

transmission through these different transmission pathways are of interest (Brookhart et al., 2002).

In this section, we examine whether β_I and β_W values are identifiable from incidence time series data alone. In particular, can solution trajectories from the SIR [i.e. $\beta_W = 0$ in system (2)] and SIWR models be distinguished from one another? This is particularly relevant given the continued use of SIR models for waterborne diseases (Koelle et al., 2005, 2006). Section 4.1 presents a fast–slow analysis of the SIWR model, which indicates that the transmission parameters will be un-identifiable when the water compartment dynamics are sufficiently fast. Section 4.2 uses parameter estimation methods to compare the SIR and SIWR models by fitting the SIR model to SIWR solution trajectories. These numerical results suggest that the transmission parameters are likely un-identifiable from incidence data even when the water compartment dynamics are slow. The results also illustrate some biological implications of incorrectly estimating the contributions from the different transmission pathways.

4.1. SIWR as a fast–slow system

It is instructive to consider (2) in the context of fast–slow systems (Jones, 1995). These are systems in which there are two natural timescales that are sufficiently different that the dynamics can be separated into fast and slow subsystems. The fast subsystem can be approximated by taking the slow variables to be constant, and the slow subsystem approximated by taking the fast variables to be in equilibrium. Analyzing the fast and slow subsystem dynamics can give insight into the dynamics of the full system.

In the SIWR model (2), the parameter ξ governs the time scale on which w evolves. Large ξ corresponds to "fast water dynamics", i.e. rapid clearance of pathogen from the water, whereas small ξ ("slow water dynamics") corresponds to situations in which pathogen persists in the water for a long time. If ξ and γ have very different magnitudes, then a separation of time scales exists and the SIWR model can be considered a fast–slow system. A fast–slow analysis of the situation where pathogen persists much longer in individuals than in the water ($\xi \gg \gamma$) gives useful insights for comparing SIR and SIWR dynamics.

A standard approximation for fast–slow systems is the quasi-steady state approximation, where the fast variables are assumed to be in equilibrium (e.g. see Segel, 1988 for a classic example). This corresponds to restricting the flow to fixed points of the fast subsystem. As in Jones (1995), we refer to the collection of fixed points of the fast subsystem as the *critical manifold*. For large ξ, the w dynamics are fast. Setting $\dot{w} = 0$ and eliminating w from system (2) gives the following equations:

$$\begin{aligned} \dot{s} &= \mu - (\beta_I + \beta_W)si - \mu s, \\ \dot{i} &= (\beta_I + \beta_W)si - \mu i - \gamma i, \\ \dot{r} &= \gamma i - \mu r. \end{aligned} \tag{29}$$

The slow flow equations (29) are exactly the standard SIR equations (4) with transmission parameter $\beta = \beta_I + \beta_W$. The critical manifold is attracting in the fast (w) subsystem of (2). Fenichel's work (Fenichel, 1971) gives the existence of an attracting manifold that is invariant for the full SIWR system and $\mathcal{O}(1/\xi)$ distance from the critical manifold. As ξ increases, the quality of the quasi-steady state approximation improves. Thus, we can only hope to identify the sum of the transmission rates $\beta_I + \beta_W$, and not the individual β_I and β_W values, when pathogen dynamics in the water compartment are sufficiently fast.

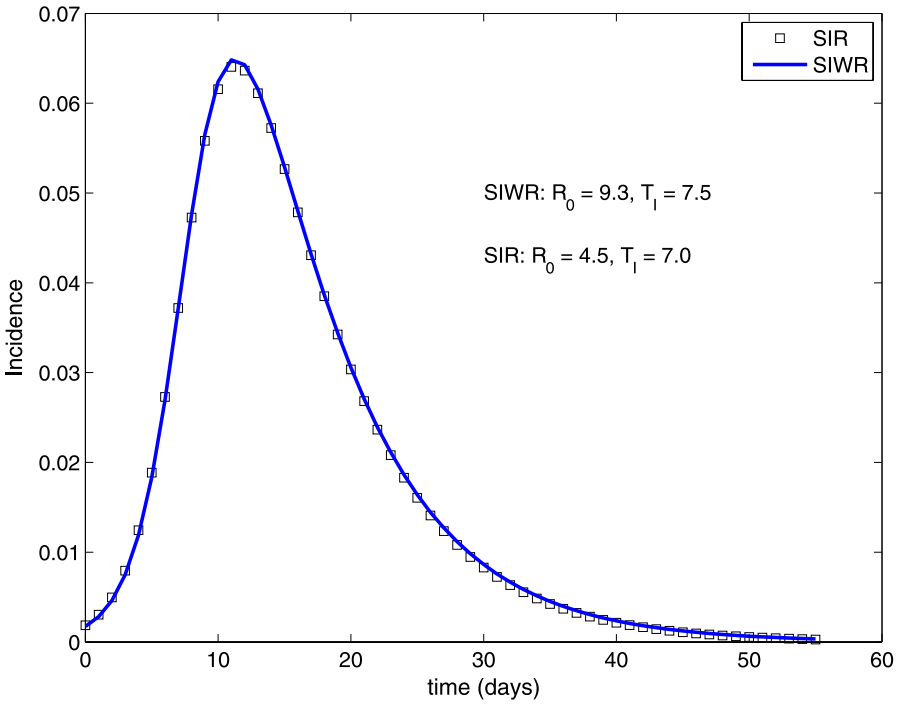

Fig. 2 Result from fitting the SIR system (4) to the SIWR system (2). Reference SIWR incidence curve $\Delta r(t)$ given by solid blue line, best fit SIR incidence curve given by black squares. SIWR parameter values: $\beta_I = 0.6217$, $\beta_W = 0.6217$, $\gamma = 0.1340$, $\xi = 0.0333$, $\mu = 0$. SIR parameter values: $\beta = 0.6509$, $\gamma = 0.1431$, $\mu = 0$. Integration time span from 0 to 56 days. Initial conditions $s_0 = 0.99$, $i_0 = 0.01$, $r_0 = 0$ in both models, and $w_0 = 0$ in the SIWR model. See Section 4.2 for parameter estimation details. (Color figure online.)

4.2. Fitting SIR to SIWR

Estimating β_I and β_W from incidence time series data may be impossible even when pathogen dynamics in the reservoir are slow. Figure 2 shows two hypothetical daily incidence curves, with one curve generated by a SIWR model, and the other by a SIR model. The two curves lie nearly on top of one another. Distinguishing between these two curves will be difficult, if not impossible, when fitting the models to data. Note that $\mathcal{R}_0$ for the SIR model is much smaller than the SIWR $\mathcal{R}_0$ value (4.5 vs. 9.3). Figure 3 shows another example of similar incidence curves for the SIR and SIWR models. In Fig. 3, the $\mathcal{R}_0$ values for the two models are similar (SIR 2.6, SIWR 2.7), but the SIR infectious period is much longer than the SIWR value (22.5 days vs. 12.6 days).

SIR and related models lacking a water compartment are often used to model waterborne diseases. Figures 2 and 3 suggest that while these models may be capable of closely fitting incidence or mortality data, the resulting fits may incorrectly estimate biologically important quantities such as $\mathcal{R}_0$ or the infectious period. To further examine this, we use Latin squares (Mckay et al., 1979; Saltelli et al., 2000) to explore the $(\mathcal{R}_0, 1/\gamma)$ parameter space in the SIWR system. Values for the basic reproductive number and infec-

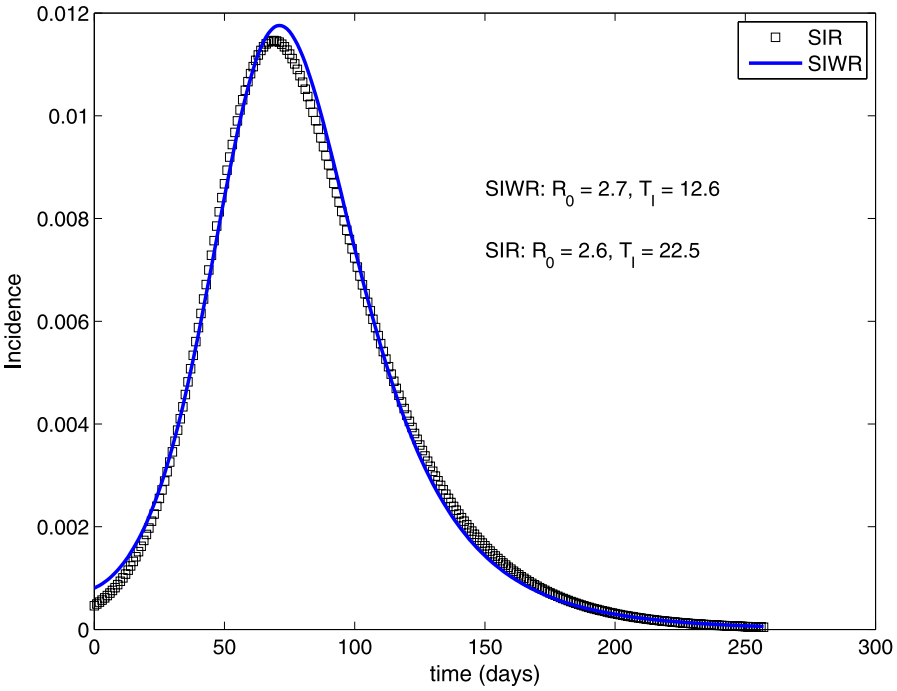

Fig. 3 Result from fitting the SIR system (4) to the SIWR system (2). Reference SIWR incidence curve $\Delta r(t)$ given by solid blue line, best fit SIR incidence curve given by black squares. SIWR parameter values: $\beta_I = 0.1072$, $\beta_W = 0.1072$, $\gamma = 0.0793$, $\xi = 0.0333$, $\mu = 0$. SIR parameter values: $\beta = 0.1176$, $\gamma = 0.0445$, $\mu = 0$. Integration time span from 0 to 258 days. Initial conditions $s_0 = 0.99$, $i_0 = 0.01$, $r_0 = 0$ in both models, and $w_0 = 0$ in the SIWR model. See Section 4.2 for parameter estimation details. (Color figure online.)

tious period were randomly selected, and a corresponding "reference" solution trajectory generated from the SIWR model. Values for $\mathcal{R}_0$ and γ were then estimated in the SIR system to best fit the reference trajectory, and the goodness of fit between the estimated SIR reproductive number and infectious period and the "true" SIWR values was examined.

4.2.1. Methods

Reference SIWR trajectories were generated by Latin square sampling from $(\mathcal{R}_0, 1/\gamma) \in [1.1, 25] \times [0.3, 30]$ (where the unit of $1/\gamma$ is days). The pathogen lifetime in the water compartment was fixed at $1/\xi = 30$ days. The fraction of the total transmission rate due to person–person transmission, $\beta_I/(\beta_I + \beta_W)$, was set to 0.5, and initial conditions were fixed at $s_0 = 0.99$, $i_0 = 0.01$, $w_0 = 0$, $r_0 = 0$. Incidence was defined as $\Delta r(t)$, the daily change in the recovered compartment. The reference trajectory time span was determined by integrating until incidence decreased below a threshold fraction of the maximum incidence. A threshold fraction of 0.005 was used throughout.

Simulated annealing (Press et al., 1992) combined with the Nelder–Mead simplex method (Nelder and Mead, 1965) was used to fit the SIR model to the reference tra-

jectories. The Nelder–Mead algorithm is a commonly used, gradient-free optimization method. In brief, an initial simplex possessing $p + 1$ vertices is specified, where p is the number of active optimization parameters. The objective function that is to be minimized is evaluated at the simplex vertices. Based upon the objective function values, new simplex vertices are chosen such that the objective function decreases. Simulated annealing uses an optimization parameter called the "temperature" to allow for optimization methods such as the Nelder–Mead algorithm to occasionally move uphill. This is done through a sequence of heating-cooling cycles. At the beginning of a cycle, the temperature is high, and parameter steps that increase the objective function are accepted relatively frequently. The temperature decreases over the heating-cooling cycle, making uphill parameter steps increasingly unlikely. Further details can be found in Press et al. (1992). Active parameters for the optimization were the transmission rate (β) and the recovery rate (γ). The objective function was least squares on the daily incidence curve $\Delta r(t)$.

A total of 175 reference trajectories were generated. One hundred heating-cooling cycles were used for each reference trajectory to estimate parameters in the SIR system. The initial simplex vertices were selected as follows. The (β, γ) parameter values that matched the SIR $\mathcal{R}_0$ and growth rate values to those of the reference trajectory were considered, together with the points $(0.1, 1)$, $(20, 10)$, and $(0.5, 0.2)$. Of these four points, the three corresponding to the smallest objective function values were chosen for the initial simplex. Termination criteria for the objective function and change in the objective function were both set to 10^{-5}. All computations were performed in `MATLAB` (source code available upon request).

4.2.2. Results

The estimated (SIR) and actual (SIWR) basic reproductive numbers and infectious periods were compared using the (natural) log of the ratio of the estimated to actual value. Positive values indicate over-estimates, and negative values under-estimates.

Let $T_I^{\text{siwr}}, T_I^{\text{sir}}$ denote the infectious period of the reference SIWR and estimated SIR models, and let $\mathcal{R}_0^{\text{siwr}}, \mathcal{R}_0^{\text{sir}}$ denote the SIWR and SIR basic reproductive numbers, respectively. Figure 4 plots $\log(\mathcal{R}_0^{\text{sir}}/\mathcal{R}_0^{\text{siwr}})$ against $\log(T_I^{\text{sir}}/T_I^{\text{siwr}})$, with the value of $\mathcal{R}_0^{\text{siwr}}$ indicated in color. The $\log(T_I^{\text{sir}}/T_I^{\text{siwr}})$ and $\log(\mathcal{R}_0^{\text{sir}}/\mathcal{R}_0^{\text{siwr}})$ values are strongly correlated, with the majority of points lying within a strip in the $\log(T_I^{\text{sir}}/T_I^{\text{siwr}}) - \log(\mathcal{R}_0^{\text{sir}}/\mathcal{R}_0^{\text{siwr}})$ plane, running roughly from $(0.1, -0.7)$ to $(0.6, 0)$. The values of $\log(T_I^{\text{sir}}/T_I^{\text{siwr}})$ and $\log(\mathcal{R}_0^{\text{sir}}/\mathcal{R}_0^{\text{siwr}})$ are furthermore strongly correlated with $\mathcal{R}_0^{\text{siwr}}$. Large $\mathcal{R}_0^{\text{siwr}}$ values tend to correspond to accurate infectious period estimates and under-estimated basic reproductive numbers. As $\mathcal{R}_0^{\text{siwr}}$ decreases, the values of $\log(\mathcal{R}_0^{\text{sir}}/\mathcal{R}_0^{\text{siwr}})$ and $\log(T_I^{\text{sir}}/T_I^{\text{siwr}})$ tend to increase. Small $\mathcal{R}_0^{\text{siwr}}$ values correspond to infectious period over-estimates.

Figure 5 further illustrates the correlation between the estimated SIR and actual SIWR reproductive number by plotting $\log(\mathcal{R}_0^{\text{sir}}/\mathcal{R}_0^{\text{siwr}})$ against $\mathcal{R}_0^{\text{siwr}}$. The Latin square sampling protocol draws parameter values for the reference SIWR trajectories from a two-dimensional space. Despite this, the plot of $\log(\mathcal{R}_0^{\text{sir}}/\mathcal{R}_0^{\text{siwr}})$ against $\mathcal{R}_0^{\text{siwr}}$ is nearly one-dimensional. Small SIWR $\mathcal{R}_0$ values are accurately estimated, while large $\mathcal{R}_0$ values are under-estimated. The ratio of estimated to actual $\mathcal{R}_0$ is roughly constant for SIWR $\mathcal{R}_0$ values larger than 7.

The SIR infectious period estimates also appear to depend heavily upon the SIWR $\mathcal{R}_0$ value. Figure 6 plots $\log(T_I^{\text{sir}}/T_I^{\text{siwr}})$ against $\mathcal{R}_0^{\text{siwr}}$. Again, the plot appears nearly one-dimensional. Small SIWR $\mathcal{R}_0$ values correspond to over-estimated infectious periods,

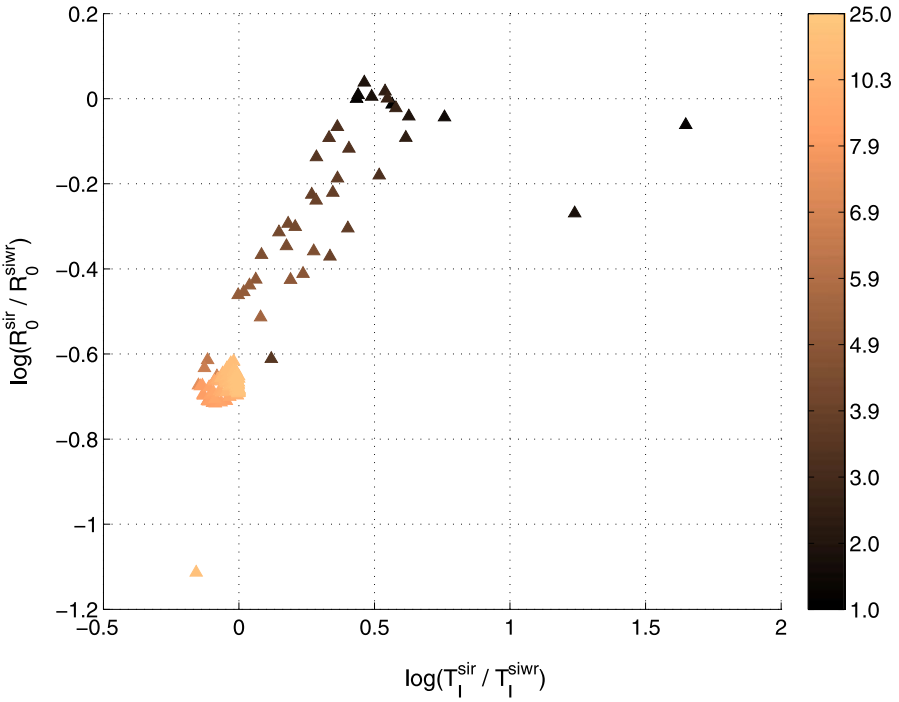

Fig. 4 Latin square and simulated annealing results from fitting the SIR system (4) to the SIWR system (2). Accuracy of the infectious period estimates $[\log(T_I^{\text{sir}}/T_I^{\text{siwr}})]$ on the x-axis, accuracy of the basic reproductive number estimates $[\log(\mathcal{R}_0^{\text{sir}}/\mathcal{R}_0^{\text{siwr}})]$ on the y-axis. Color of the plotted points indicates the value of $\mathcal{R}_0^{\text{siwr}}$. See Section 4.2. (Color figure online.)

while large $\mathcal{R}_0$ values correspond to accurate infectious period estimates. For $\mathcal{R}_0 > 5$, the estimated infectious periods are accurate to within 14%.

Basic reproductive number under-estimates Large $\mathcal{R}_0^{\text{siwr}}$ values correspond to accurate SIR estimates of the infectious period, but under-estimates of the basic reproductive number (Figs. 4–6). To understand this, first note that while the final outbreak size Z is determined by the basic reproductive number [cf., (27)], Z is relatively insensitive to $\mathcal{R}_0$ when $\mathcal{R}_0$ is large. There is thus greater allowance for incorrectly estimating the basic reproductive number when $\mathcal{R}_0^{\text{siwr}}$ is large, as a decent match to the final outbreak size may still occur despite the incorrect $\mathcal{R}_0$ estimate. For large $\mathcal{R}_0$, the proportion of the population that is susceptible at peak incidence is small. In this situation, the decreasing portion of the incidence curve is largely due to transfer of individuals to the recovered (r) compartment who are already infected at the time of peak incidence. This transfer rate is determined by the infectious period. Provided there is a good fit to the peak incidence amplitude, the SIR estimate of the infectious period will thus tend to be accurate. From Proposition 1, we know that if the infectious periods and growth rates of the SIR and SIWR models match, then the SIR $\mathcal{R}_0$ value will be less than or equal to the SIWR $\mathcal{R}_0$ value.

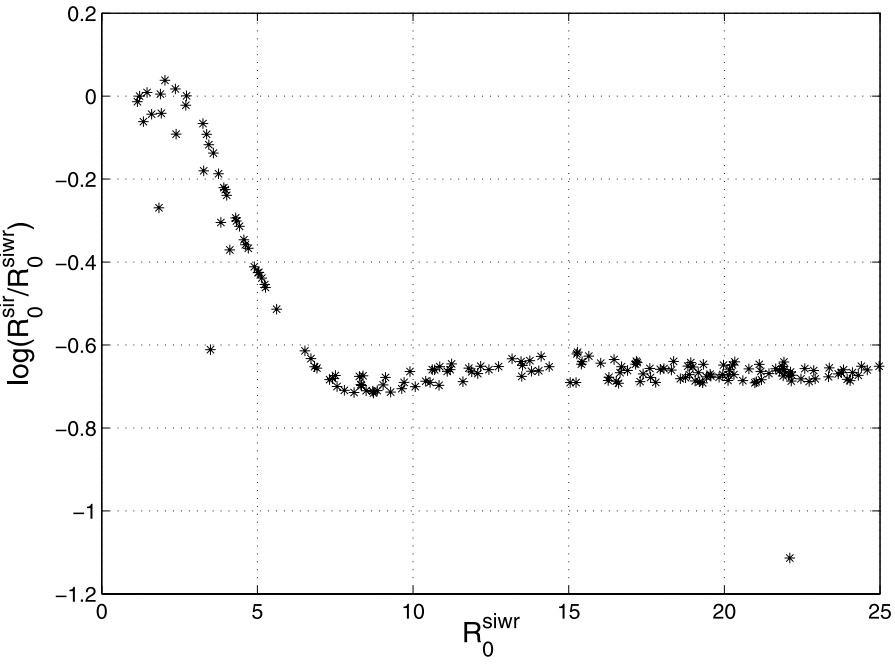

Fig. 5 Latin square and simulated annealing results from fitting the SIR system (4) to the SIWR system (2). Accuracy of the basic reproductive number estimates $[\log(\mathcal{R}_0^{\text{sir}}/\mathcal{R}_0^{\text{siwr}})]$ plotted against $\mathcal{R}_0^{\text{siwr}}$. Note that the plot is nearly one dimensional, despite Latin square sampling from a two dimensional space. See Section 4.2.

Infectious period over-estimates The infectious period in the SIR system is over-estimated when $\mathcal{R}_0^{\text{siwr}}$ is small. To understand this, note that the final outbreak size is increasingly sensitive to $\mathcal{R}_0$ as $\mathcal{R}_0$ decreases. When $\mathcal{R}_0$ is small, a good estimate of $\mathcal{R}_0$ is important for obtaining a reasonable least squares fit to the incidence curve. The SIR infectious period needed to match both $\mathcal{R}_0$ and the growth rate in the SIWR model is $T_I^{\text{siwr}}[1 + T_W(\lambda - \tilde{\lambda})]$. As $\lambda \geq \tilde{\lambda}$ [cf., (11)], matching the basic reproductive number and growth rate leads to an over-estimate of the true infectious period.

Outliers Three outliers are apparent in Fig. 4. The outlier in the lower left of the figure (with $\log(\mathcal{R}_0^{\text{sir}}/\mathcal{R}_0^{\text{siwr}}) < -1$) corresponds to a rapid outbreak which is over after 3 days. The daily incidence measurements used in the objective function are too widely spaced for such a brief outbreak. Using a finer time resolution for the incidence curve removes this outlier. The remaining two outliers in the upper right of the figure ($\log(T_I^{\text{sir}}/T_I^{\text{siwr}}) > 1$) correspond to poor SIR fits to the SIWR trajectories. These fits can be greatly improved by including the initial conditions as active optimization parameters, or by using an SEIR rather than an SIR model. A thorough examination of how $\mathcal{R}_0$ and infectious period estimates are affected by the initial conditions and number of infected compartments in the model is an area for future work.

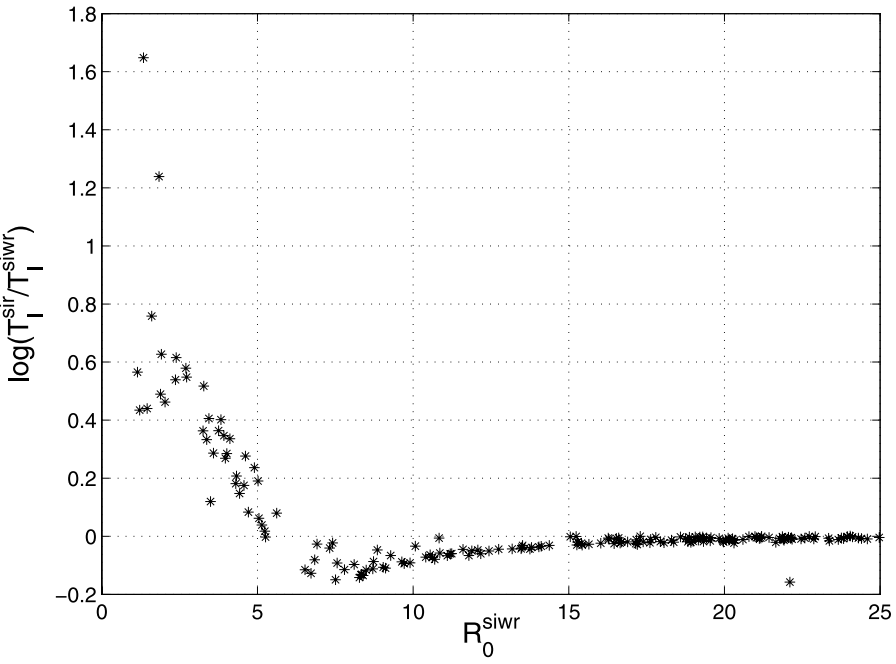

Fig. 6 Latin square and simulated annealing results from fitting the SIR system (4) to the SIWR system (2). Accuracy of the infectious period estimates $[\log(T_I^{\text{sir}}/T_I^{\text{siwr}})]$ plotted against $\mathcal{R}_0^{\text{siwr}}$. Note that the plot is nearly one dimensional, despite Latin square sampling from a two dimensional space. See Section 4.2.

5. Discussion

Multiple transmission routes are a ubiquitous feature of waterborne diseases. The SIWR model (2) provides an ODE framework for examining how these transmission routes influence disease dynamics. The analysis presented here illustrates how multiple transmission routes and persistence in a reservoir outside of human hosts can affect fundamental characteristics such as the basic reproductive number and epidemic growth rate. Estimates of $\mathcal{R}_0$ and infectious period can be sensitive to the relative contributions of the different transmission pathways and the pathogen lifetime in the water. This sensitivity is relevant for dynamical studies of waterborne diseases because basic life history and epidemiological traits remain uncertain for many waterborne pathogens. Previous studies have emphasized the roles of asymptomatic infection (Eisenberg et al., 2002; King et al., 2008), length of infection-derived immunity (King et al., 2008), long term disease carriers (Cvjetanovic et al., 1978), and hyper-infectious pathogen states (Hartley et al., 2006) on waterborne disease dynamics. This paper indicates the importance of also considering multiple transmission pathways.

In the SIWR model (2), an infected individual generates secondary infections both through direct contact with susceptible individuals, as well as by pathogen shedding into the water compartment. Disease transmission through the water can be thought of as a delayed transmission route, as pathogens must first pass through the water compartment

before reaching a susceptible host. Considering person–water–person transmission in this way gives an intuitive understanding of our finding that when $\mathcal{R}_0$ is fixed, increasing the relative contribution of person–water–person transmission results in a slower growth rate (Proposition 2). We can think of an infected individual as having an effective infectious period which takes into account both person–person and person–water–person transmission. This effective infectious period increases as the relative contribution of waterborne transmission increases. In order for $\mathcal{R}_0$ to be fixed, the epidemic growth rate must decrease to compensate. Similarly, regarding waterborne transmission as a delayed transmission route gives insight into our finding that using an SIR instead of an SIWR model can lead to over-estimates of the infectious period. This is the expected result if the true infectious period in the SIR model were replaced with the longer, effective infectious period which accounts for waterborne transmission.

The model and analysis presented here concern the simple case where both the infectious period and pathogen lifetime in the water are exponentially distributed. These assumptions are likely to be unrealistic for many diseases. Examining the effect of non-exponentially distributed infectious periods and pathogen lifetimes in the water on the results presented in this paper is an area for future work.

The SIWR model is a general framework that can be adapted for different specific diseases. Whether the distinction made in the SIWR model between person–person and person–water–person transmission is important depends upon the length of time that the pathogen in question can persist in the water compartment. This will vary between pathogen types, and depend upon environmental conditions such as temperature, salinity, pH, and light (King and Monis, 2007; Thomas et al., 1999). Decay rates are often quite slow, with survival times of up to several months reported for *Giardia* (Flanagan, 1992), *Cryptosporidium* (Robertson et al., 1992), and *Campylobacter* (Rollins and Colwell, 1986; Thomas et al., 1999). Pathogens such as *Campylobacter*, *E. coli*, and *V. cholerae* can also enter non-culturable but viable life stages, which have still slower decay rates (Rollins and Colwell, 1986; Xu et al., 1982). Permanent environmental reservoirs exist for some species. One such example is *V. cholerae* persisting indefinitely in marine and estuarine environments in association with plankton (Tamplin et al., 1990).

Many different specific transmission pathways may exist for a given disease. How these pathways fit into the person–person and person–water–person pathways in the SIWR framework—and whether changes to this framework are needed—will depend upon the time scales associated with the different pathways. For example, it is reasonable to include food-borne transmission associated with infected food handlers into the person–person pathway if the pathogen decay rate in the food is rapid. On the other hand, if the pathogen decay rate in food or on door and tap handles is slow, as may be the case for norovirus (Barker et al., 2004; Duizer and Koopmans, 2006), then additional compartments in the model may be necessary. Permanent environmental pathogen reservoirs are another important consideration. Introducing background reservoir transmission into the SIWR model, such as the reservoir-person transmission term in King et al. (2008), may be suitable for pathogens such as *V. cholerae*.

Environmental factors and ecological interactions play important roles in waterborne disease dynamics. The SIWR framework provides a convenient starting point for exploring possible mechanisms by which different environmental and ecological factors affect disease dynamics. Pathogen dynamics in the water compartment of (2) can be modified

to reflect interactions between different pathogen strains (Koelle et al., 2006), interactions with other species (e.g. *V. cholerae* and bacteriophage (Jensen et al., 2006) or copepods (Tamplin et al., 1990)), external pathogen inputs such as run-off, which may be affected by rainfall or other weather conditions (Auld et al., 2004; Curriero et al., 2001; Jones, 2001), seasonal conditions in the water reservoir (King et al., 2008), and variations in climate such as El Niño (Pascual et al., 2000). Agricultural land use and eutrophication are also concerns (Wu, 1999).

Estimating the extent to which different transmission pathways contribute to a disease outbreak is challenging. Our comparison of the SIR and SIWR models indicates that separating the contributions from person–person and person–water–person transmission in the SIWR model may be impossible from incidence data alone. Brookhart et al. (2002) similarly found that the degree of person–person transmission could not be confidently estimated from incidence data for the 1993 Milwaukee *Cryptosporidium* outbreak without knowing the extent of asymptomatic infections. Time series data on pathogen levels in environmental water sources could be helpful for estimating transmission parameters for the different pathways, provided that pathogen infectivity while in the water is known. Environmental pathogen measurements would also be valuable for examining spatial spread of waterborne disease outbreaks.

Acknowledgements

We thank Jonathan Dushoff for valuable discussions and comments on an earlier draft, and Susan Marsh-Rollo for making Figs. 1 and A.1. D.J.D.E. is supported by the J. S. McDonnell Foundation, NSERC and CIHR.

Appendix: Multi-stage generalization

In this Appendix, we present model equations for extending system (1) to include n infected compartments. We refer to the resulting model as the SI^{n}WR system. We compute the basic reproductive number of the SI^{n}WR model, and show that the final outbreak size relation (27) holds for this system.

A.1 SI^{n}WR model equations

Figure A.1 shows the flow diagram for an extension of system (1) to include n infected compartments. The corresponding system of differential equations is given below:

$$\begin{aligned}
\dot{S} &= \mu N - b_W S W - \sum_k b_{I_k} S I_k - \mu S, \\
\dot{I}_1 &= b_W S W + \sum_k b_{I_k} S I_k - \gamma_1 I_1 - \mu I_1, \\
&\vdots \\
\dot{I}_k &= \gamma_{k-1} I_{k-1} - \gamma_k I_k - \mu I_k,
\end{aligned} \tag{A.1}$$

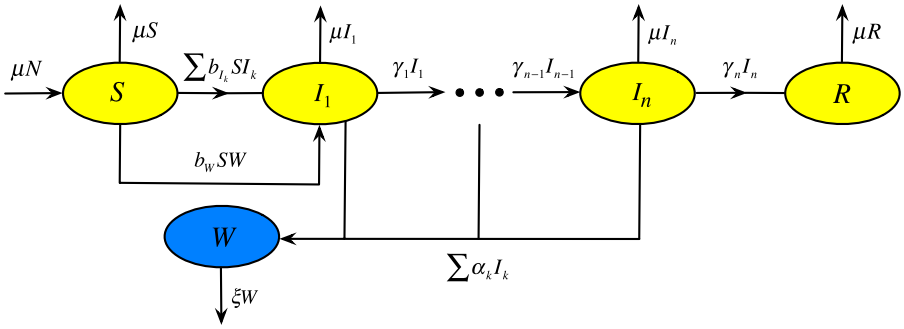

Fig. A.1 Flow diagram for the SI^{n}WR model (A.1). See Tables 1–2.

$$\begin{aligned}
&\vdots\\
\dot{W} &= \sum_k \alpha_k I_k - \xi W,\\
\dot{R} &= \gamma_n I_n - \mu R.
\end{aligned}$$

Note that distinct parameters exist for the person–person transmission rate (b_{I_k}), person–water pathogen shedding rate (α_k), and decay rate (γ_k) for each infected compartment.

Introducing non-dimensional variables $s = S/N, i_k = I_k/N, r = R/N, w = \frac{\xi}{N\sum_k \alpha_k} W$, and scaled transmission and shedding parameters $\beta_{I_k} = b_{I_k} N$, $\beta_{W_k} = b_W N \alpha_k/\xi$, and $a_k = \alpha_k/\sum_j \alpha_j$, gives the following scaled system:

$$\begin{aligned}
\dot{s} &= \mu - sw\sum_k \beta_{W_k} - s\sum_k \beta_{I_k} i_k - \mu s,\\
\dot{i}_1 &= sw\sum_k \beta_{W_k} + s\sum_k \beta_{I_k} i_k - \gamma_1 i_1 - \mu i_1,\\
&\vdots\\
\dot{i}_k &= \gamma_{k-1} i_{k-1} - \gamma_k i_k - \mu i_k\\
&\vdots\\
\dot{w} &= \xi\left(\sum_k a_k i_k - w\right),\\
\dot{r} &= \gamma_n i_n - \mu r.
\end{aligned} \tag{A.2}$$

The scaled pathogen shedding parameters a_k are normalized versions of the α_k, such that $\sum_k a_k = 1$. The $\dot{w}$ term in system (A.2) involves a weighted average of the i_k, with weights given by a_k.

It is convenient to let $\beta_W = \sum \beta_{W_k}$. Then we have $\beta_{W_k} = a_k \beta_W$.

A.2 Basic reproductive number

As in Section 3.1, let FV^{-1} denote the next generation matrix at the disease free equilibrium (van den Driessche and Watmough, 2002). For system (A.2), the rate of new

infections corresponds to

$$F = \begin{pmatrix} \beta_{I_1} & \cdots & \beta_{I_n} & \beta_W \\ 0 & & & \\ & \ddots & \ddots & \\ & & & 0 \end{pmatrix}. \tag{A.3}$$

The matrix of expected residence times $V^{-1} \in \mathbb{R}^{(n+1)\times(n+1)}$ is computed from V, whose entries correspond to transition rates for the disease compartments:

$$V = \begin{pmatrix} \gamma_1 + \mu & & & & & \\ -\gamma_1 & \gamma_2 + \mu & & & & \\ & -\gamma_2 & \gamma_3 + \mu & & & \\ & & \ddots & \ddots & & \\ & & & -\gamma_{n-1} & \gamma_n + \mu & \\ -\xi a_1 & -\xi a_2 & \cdots & -\xi a_{n-1} & -\xi a_n & \xi \end{pmatrix}. \tag{A.4}$$

See van den Driessche and Watmough (2002) for details.

Let $\tilde{V}^{-1}$ denote the upper left $n \times n$ block of V^{-1}. The entries of $\tilde{V}^{-1}$ are given by

$$\tilde{V}^{-1}_{ij} = \begin{cases} 0, & i < j, \\ 1/(\gamma_i + \mu), & i = j, \\ \frac{\prod_{k=j}^{i-1} \gamma_k}{\prod_{k=j}^{i} (\gamma_k + \mu)}, & i > j. \end{cases} \tag{A.5}$$

The entries of the last row of V^{-1} are

$$V^{-1}_{n+1,j} = \begin{cases} \sum_{k=j}^{n} a_k \tilde{V}^{-1}_{kj} & 1 \le j \le n, \\ 1/\xi & j = n+1. \end{cases} \tag{A.6}$$

The basic reproductive number corresponds to the $(1, 1)$ entry of FV^{-1}:

$$\begin{aligned} \mathcal{R}_0 &= \rho\left(FV^{-1}\right) \\ &= \sum_{j=1}^{n} \beta_{I_j} \tilde{V}^{-1}_{j,1} + \beta_W \sum_{j=1}^{n} a_j \tilde{V}^{-1}_{j,1} \\ &= \sum_{j=1}^{n} \beta_{I_j} \tilde{V}^{-1}_{j,1} + \sum_{j}^{n} \beta_{W_j} \tilde{V}^{-1}_{j,1} \\ &= \sum_{j=1}^{n} (\beta_{I_j} + \beta_{W_j}) \tilde{V}^{-1}_{j,1} \\ &= \frac{\beta_{I_1} + \beta_{W_1}}{\gamma_1 + \mu} + (\beta_{I_2} + \beta_{W_2}) \frac{\gamma_1}{(\gamma_1 + \mu)(\gamma_2 + \mu)} + \cdots \\ &\quad + (\beta_{I_n} + \beta_{W_n}) \frac{\gamma_1 \cdots \gamma_{n-1}}{(\gamma_1 + \mu) \cdots (\gamma_n + \mu)}. \end{aligned} \tag{A.7}$$

In the case where $\mu = 0$, we have the following expression for the basic reproductive number for system (A.2):

$$\mathcal{R}_0 = \sum_{k=1}^{n} \frac{\beta_{I_k} + \beta_{W_k}}{\gamma_k}. \tag{A.8}$$

A.3 Final outbreak size

The final outbreak size relation (27) holds for the SI^{n}WR system (A.2) when $\mu = 0$ and $\mathcal{R}_0 > 1$. To see this, first note that when $\mu = 0$, the disease "burns out" as in the SIWR system (2). The proof is essentially the same as for Lemma 2, so we omit it here. The following proposition proves the final outbreak size relation for a newly invading pathogen for system (A.2), using the approach of Ma and Earn (2006).

Proposition A.1. *Let $\mu = 0$ and $\mathcal{R}_0 > 1$ for system (A.2). Let s_0 denote the initial susceptible proportion, and w_0 the initial pathogen level in the water. In the limit $s_0 \to 1$, $w_0 \to 0$, the final outbreak size in system (A.2) approaches the solution Z to the final outbreak size relation (27).*

Proof: Let $G_k(t) = \sum_{j=k+1}^{n} i_j(t) + r(t)$ for $k = 1, \ldots, n-1$, and let $G_n(t) = r(t)$. Then we have $\dot{G}_k = \gamma_k i_k$ for $k = 1, \ldots, n$.

Let

$$F(t) = \log s(t) + \sum_{k=1}^{n} G_k(t) \frac{\beta_{W_k} + \beta_{I_k}}{\gamma_k} - \frac{1}{\xi} \beta_W w(t). \tag{A.9}$$

Recall that $\beta_W = \sum \beta_{W_k}$. Differentiating F with respect to time gives

$$\begin{aligned} \dot{F} &= \sum_{k=1}^{n} \beta_{W_k} i_k - \beta_W \sum_{k=1}^{n} a_k i_k \\ &= \sum_{k=1}^{n} \beta_{W_k} i_k - \sum_{k=1}^{n} a_k \beta_W i_k \\ &= \sum_{k=1}^{n} \beta_{W_k} i_k - \sum_{k=1}^{n} \beta_{W_k} i_k \\ &= 0. \end{aligned} \tag{A.10}$$

Thus, F is constant along solution trajectories. As $t \to \infty$, $r(t)$ increases to a limit $\bar{r}$. As the disease burns out, $i_k(t) \to 0$ for $k = 1, \ldots, n$, giving that $G_k \to \bar{r}$ for each k. As $i_k(t) \to 0$ for each k, we also have that $s(t) \to 1 - \bar{r}$. Disease burnout gives that $w(t) \to 0$ as well. Setting $F(0) = \lim_{t \to \infty} F(t)$, we then have

$$\log s_0 + \sum_{k=1}^{n} G_k(0) \frac{\beta_{W_k} + \beta_{I_k}}{\gamma_k} - \frac{1}{\xi} \beta_W w_0 = \log(1 - \bar{r}) + \bar{r} \sum_{k=1}^{n} \frac{\beta_{W_k} + \beta_{I_k}}{\gamma_k}. \tag{A.11}$$

Now let $s_0 \to 1, w_0 \to 0$ in (A.11). Note that $s_0 \to 1$ forces r_0 and $i_k(0)$ to approach 0, which in turn means that $G_k(0) \to 0$ for each k. As $r_0 \to 0$, $\bar{r}$ approaches the final outbreak size Z. Finally, substituting the expression (A.8) for $\mathcal{R}_0$ when $\mu = 0$ gives the desired final outbreak size relation (27). □

References

Andersen, M.D., Neumann, N.F., 2007. *Giardia intestinalis*: new insights on an old pathogen. Rev. Med. Microbiol. 18(2), 35–42.

Anderson, R., Watson, R., 1980. On the spread of a disease with gamma distributed latent and infectious periods. Biometrika 67(1), 191–198.

Anderson, R.M., May, R.M., 1991. Infectious Diseases of Humans: Dynamics and Control. Oxford University Press, Oxford.

Ashbolt, N., 2004. Microbial contamination of drinking water and disease outcomes in developing regions. Toxicology 198, 229–238.

Auld, H., MacIver, D., Klaassen, J., 2004. Heavy rainfall and waterborne disease outbreaks: the Walkerton example. J. Toxicol. Environ. Health A 67, 1879–1887.

Barker, J., Vipond, I., Bloomfield, S., 2004. Effects of cleaning and disinfection in reducing the spread of norovirus contamination via environmental surfaces. J. Hosp. Infect. 58, 42–49.

Brookhart, M.A., Hubbard, A., van der Laan, M.J., Colford, J., Eisenberg, J.N.S., 2002. Statistical estimation of parameters in a disease transmission model: analysis of a *Cryptosporidium* outbreak. Stat. Med. 21(23), 3627–3638.

Butzler, J., 2004. Campylobacter, from obscurity to celebrity. Clin. Microbiol. Infect. 10(10), 868–876.

Codeco, C., 2001. Endemic and epidemic dynamics of cholera: the role of the aquatic reservoir. BMC Infect. Dis. 1.

Curriero, F., Patz, J., Rose, J., Lele, S., 2001. The association between extreme precipitation and waterborne disease outbreaks in the United States, 1948–1994. Am. J. Public Health 91, 1194–1199.

Cvjetanovic, B., Grab, B., Uemura, K., 1978. Dynamics of acute bacterial diseases, epidemiological models and their application to public health. Bull. World Health Organ. 56(S1), 1–143.

Duizer, E., Koopmans, M., 2006. Tracking foodborne viruses: lessons from noroviruses. In: Motarjemi, Y., Adam, M. (Eds.), Emerging Foodborne Pathogens, pp. 77–110. CRC Press, Boca Raton.

Eisenberg, J.N., Brookhart, M., Rice, G., Brown, M., Colford, J., 2002. Disease transmission models for public health decision making: analysis of epidemic and endemic conditions caused by waterborne pathogens. Environ. Health Perspect. 110(8), 783–790.

Eisenberg, J.N., Lewis, B.L., Porco, T.C., Hubbard, A.H., Colford, J.M. Jr., 2003. Bias due to secondary transmission in estimation of attributable risk from intervention trials. Epidemiology 14(4), 442–450.

Faruque, S., Albert, M., Mekalanos, J., 1998. Epidemiology, genetics, and ecology of toxigenic *Vibrio cholerae*. Microbiol. Mol. Biol. Rev. 62(4), 1301–1314.

Faruque, S., Islam, M., Ahmad, Q., Faruque, A.S.G., Sack, D., Nair, G., Mekalanos, J., 2005. Self-limiting nature of seasonal cholera epidemics: role of host-mediated amplification of phage. Proc. Natl. Acad. Sci. USA 102(17), 6119–6124.

Fenichel, N., 1971. Persistence and smoothness of invariant manifolds for flows. Indiana Univ. Math. J. 21(3), 193–226.

Flanagan, P., 1992. Giardia—diagnosis, clinical course and epidemiology. A review. Epidemiol. Infect. 109(1), 1–22.

Ford, T., 1999. Microbiological safety of drinking water: United States and global perspectives. Environ. Health Perspect. 107(Suppl. 1), 191–206.

Gerba, C., Rose, J., Haas, C., Crabtree, K., 1996. Waterborne rotavirus: a risk assessment. Water Res. 30, 2929–2940.

Goh, K., Teo, S., Lam, S., Ling, M., 1990. Person-to-person transmission of cholera in a psychiatric hospital. J. Infect. 20(3), 193–2000.

Guckenheimer, J., Holmes, P., 1983. Nonlinear Oscillations, Dynamical Systems, and Bifurcations of Vector Fields. Springer, Berlin.

Hartley, D., Morris, J., Smith, D., 2006. Hyperinfectivity: a critical element in the ability of *V. cholerae* to cause epidemics? PLoS Med. 3, 63–69.

Hirsch, M.W., Smale, S., 1974. Differential Equations, Dynamical Systems, and Linear Algebra. Academic Press, New York.
Hunter, P., Waite, M., Ronchi, E. (Eds.), 2003. Drinking Water and Infectious Disease: Establishing the Links. CRC Press, Boca Raton.
Hyman, J.M., Li, J., Ann Stanley, E., 1999. The differential infectivity and staged progression models for the transmission of HIV. Math. Biosci. 155, 77–109.
Jensen, M., Faruque, S., Mekalanos, J., Levin, B., 2006. Modeling the role of bacteriophage in the control of cholera outbreaks. Proc. Natl. Acad. Sci. USA 103(12), 4652–4657.
Jones, C.K., 1995. Geometric singular perturbation theory. In: Lecture Notes in Mathematics, vol. 1609, pp. 44–118. Springer, Berlin.
Jones, K., 2001. Campylobacters in water, sewage and the environment. J. Appl. Microbiol. 90(S6), 68S–79S.
Karanis, P., Kourenti, C., Smith, H., 2007. Waterborne transmission of protozoan parasites: a worldwide review of outbreaks and lessons learnt. J. Water Health 5(1), 1–38.
Kermack, W.O., McKendrick, A.G., 1927. A contribution to the mathematical theory of epidemics. Proc. R. Soc. Lond. A 115, 700–721.
King, A.A., Ionides, E.L., Pascual, M., Bouma, M.J., 2008. Inapparent infections and cholera dynamics. Nature 454, 877–880.
King, B., Monis, P., 2007. Critical processes affecting *Cryptosporidium* oocyst survival in the environment. Parasitology 134, 309–323.
Koelle, K., Pascual, M., Yunus, M., 2005. Pathogen adaptation to seasonal forcing and climate change. Proc. R. Soc. Lond. B 272, 971–977.
Koelle, K., Pascual, M., Yunus, M., 2006. Serotype cycles in cholera dynamics. Proc. R. Soc. Lond. B 273, 2879–2886.
Korobeinikov, A., 2004. Lyapunov functions and global properties for SEIR and SEIS epidemic models. Math. Med. Biol. 21, 75–83.
Korobeinikov, A., Wake, G., 2002. Lyapunov functions and global stability for SIR, SIRS, and SIS epidemiological models. Appl. Math. Lett. 15, 955–961.
LaSalle, J., Lefschetz, S., 1961. Stability by Liapunov's Direct Method. Academic Press, New York.
Leclerc, H., Schwartzbrod, L., Dei-Cas, E., 2002. Microbial agents associated with waterborne diseases. Crit. Rev. Microbiol. 28(4), 371–409.
Ma, J., Earn, D., 2006. Generality of the final size formula for an epidemic of a newly invading infectious disease. Bull. Math. Biol. 68, 679–702.
Marshall, M., Naumovitz, D., Ortega, Y., Sterling, C., 1997. Waterborne protozoan pathogens. Clin. Microbiol. Rev. 10(1), 67–85.
Mckay, M., Beckman, R., Conover, W., 1979. Comparison of 3 methods for selecting values of input variables in the analysis of output from a computer code. Technometrics 21(2), 239–245.
Nasser, A., 1994. Prevalence and fate of hepatitis A virus in water. Crit. Rev. Environ. Sci. Technol. 24(4), 281–323.
Nelder, J., Mead, R., 1965. A simplex method for function minimization. Comput. J. 7, 308–313.
Pascual, M., Rodo, X., Ellner, S.P., Colwell, R., Bouma, M.J., 2000. Cholera dynamics and El Niño-Southern oscillation. Science 289, 1766–1769.
Press, W.H., Teukolsky, S.A., Vetterling, W.T., Flannery, B.P., 1992. Numeric Recipes in C: The Art of Scientific Computing, 2nd edn. Cambridge University Press, New York.
Prüss-Üstün, A., Bos, R., Gore, F., Bartram, J., 2008. Safer Water, Better Health: Costs, Benefits and Sustainability of Interventions to Protect and Promote Health. World Health Organization, Geneva.
Robertson, L., Campbell, A., Smith, H., 1992. Survival of *Cryptosporidium* oocysts under various environmental pressures. Appl. Environ. Microbiol. 58, 3494–3500.
Rollins, D., Colwell, R., 1986. Viable but nonculturable stage of *Campylobacter jejuni* and its role in survival in the natural aquatic environment. Appl. Environ. Microbiol. 52, 531–538.
Rose, J., 1997. Environmental ecology of *Cryptosporidium* and public health implications. Annu. Rev. Public Health 18, 135–161.
Sack, D., Sack, R., Nair, G., Siddique, A., 2004. Cholera. Lancet 363, 223–233.
Saltelli, A., Chan, K., Scott, E., 2000. Sensitivity Analysis. Wiley, New York.
Schuster, C., Ellis, A., Robertson, W., Charron, D., 2005. Infectious disease outbreaks related to drinking water in Canada, 1974–2001. Can. J. Public Health 96(4), 254–258.
Segel, L., 1988. On the validity of the steady state assumption of enzyme kinetics. Bull. Math. Biol. 50, 579–593.

Snow, J., 1936. Snow on Cholera: Being a Reprint of Two Papers. The Commonwealth Fund, New York.
Tamplin, M., Gauzens, A., Huq, A., Sack, D., Colwell, R., 1990. Attachment of *Vibrio cholerae* serogroup-O1 to zooplankton and phytoplankton of Bangladesh waters. Appl. Environ. Microbiol. 56(6), 1977–1980.
Thomas, C., Hill, D., Mabey, M., 1999. Evaluation of the effect of temperature and nutrients on the survival of *Campylobacter* spp. in water microcosms. J. Appl. Microbiol. 86(6), 1024–1032.
van den Driessche, P., Watmough, J., 2002. Reproduction numbers and sub-threshold endemic equilibria for compartmental models of disease transmission. Math. Biosci. 180, 29–48.
Wagner, B.G., Earn, D., 2010. Population dynamics of live-attenuated virus vaccines. Theor. Popul. Biol., in press.
Wallinga, J., Lipsitch, M., 2007. How generation intervals shape the relationship between growth rates and reproductive numbers. Proc. R. Soc. B 274, 599–604.
WHO, 2009. Cholera: global surveillance summary, 2008. Wkly. Epidemiol. Rec. 84, 309–324.
Wu, R., 1999. Eutrophication, water borne pathogens and xenobiotic compounds: environmental risks and challenges. Mar. Pollut. Bull. 39, 11–22.
Xu, H., Roberts, N., Singleton, F., Attwell, R., Grimes, D., Colwell, R., 1982. Survival and viability of nonculturable *Escherichia coli* and *Vibrio cholerae* in the estuarine and marine environment. Microb. Ecol. 8, 313–323.